Thermostructural shape memory effect observations of ductile Cu-Al-Mn smart alloy

Canan Aksu Canbay[*1], Oktay Karaduman [1b],
Pshdar A. Ibrahim [1c] and İskender Özkul [2a]

[1] *Department of Physics, Firat University, 23119 Elazig Center, Elazig, Turkey*
[2] *Department of Mechanical Engineering, Mersin University, 3334 Yenişehir, Mersin, Turkey*

Abstract. The Cu-Al-Mn shape memory alloy (SMA) with a new different composition was fabricated by arc melting method. The characteristic shape memory effect (SME) property of Cu-Al based SMA was revealed by performing thermostructural measurements. The differential scanning calorimetry (DSC) tests were taken to observe the reversible martensitic phase transformation peaks of the alloy as evidence of SME property of the alloy. To determine the basic thermodynamical parameters of the alloy, these endothermic and exothermic transformation peaks were analyzed by the tangent differentiation method that was performed automatically by the DSC analyzing program over a manually selected part on the DSC curve and by these analyses the characteristic martensitic transformation temperatures (working temperatures) that found below 100°C and the enthalpy change values of the alloy were directly obtained. The other kinetic transformation parameters of the alloy - the entropy change, hysteresis, and equilibrium temperature - were also determined. The common high-temperature behavior of the Cu-Al based Heusler alloys was detected by differential thermal analysis (DTA) measurement. The XRD and metallography tests that were conducted at room temperature showed the presence of M18R and the dominant 2H martensite structures that formed in the alloy and this dual martensitic structure was also prescribed by determining the theoretical *e/a* ratio of the alloy. Furthermore, the microhardness tests on the alloy demonstrated the high ductility feature of the alloy. All results demonstrated that the CuAlMn alloy exhibiting a shape memory effect property can be useful in smart alloy applications.

Keywords: shape memory alloy; CuAlMn Heusler alloy; ductility; entropy; shape memory effect; martensite; DSC; DTA; XRD; optical metallography

1. Introduction

Area of shape memory alloys (SMAs) is a major area of interest within the field of smart materials. SMAs are special materials capable of creating large deformations than returning to a predefined form while unloading or overheating (Otsuka and Wayman 1998). The shape memory mechanism or shape memory effect (SME) is based on martensitic transformation which is a reversible solid to solid reaction from high symmetry & temperature austenite phase to low

---

*Corresponding author, Associate Professor, E-mail: caksu@firat.edu.tr
[a] Associate Professor, E-mail: iskender@mersin.edu.tr
[b] Ph.D. Student, E-mail: o.karaduman@firat.edu.tr; okinist@hotmail.com
[c] M.Sc. Student, E-mail: pshdaribrahim018@gmail.com

symmetry & temperature martensite phase and vice versa (Otsuka and Wayman 1998, Canbay *et al.* 2014a, Canbay and Karagoz 2013). SMAs that exhibit a shape change by their SME property only upon heating (one-way shape memory effect or OWSME) are named as one-way shape memory alloys (OWSMAs). Sometimes, upon recooling, they also show an extra second shape change (two-way shape memory effect, TWSME) which are called two-way shape memory alloys (TWSMAs) (Otsuka and Wayman 1998). Recent developments in material science have contributed to a multitude of studies that include multiple uses of SMAs. The SME and the superelasticity (SE) properties also affected the usage of the memory alloys to meet the capacity of applications (Canbay and Aydoğdu 2013, Oliveira *et al.* 2019) through a diverse range of sectors, such as medical (Canbay and Karagoz 2013, Oliveira *et al.* 2019, Özkul *et al.* 2019, Canbay and Keskin 2014, Xie *et al.* 2015) aerospace, (Oliveira *et al.* 2019, Özkul *et al.* 2019, Xie *et al.* 2015) aerospace machinery (Özkul *et al.* 2019), electronics (Özkul *et al.* 2019, Xie *et al.* 2015) and civil construction (Oliveira *et al.* 2019, Özkul *et al.* 2019, Xie *et al.* 2015).

The most well established SMAs are NiTi and Cu-based binary and ternary systems (Canbay and Karagoz 2013, Canbay and Keskin 2014). Cu-based SMAs have some new advances such as excellent damping, better electrical and thermal conductivity than NiTi ones, and improved microstructural control during alloy development which enhances their mechanical properties (Canbay *et al.* 2014a, Oliveira *et al.* 2019). But, Cu-based SMAs are the alloys most under 'hunting' mainly due to their easer fabrication (in some ways) and lower prices (Canbay and Karagoz 2013, Canbay and Aydoğdu 2013, Oliveira *et al.* 2019, Özkul *et al.* 2019, Canbay and Keskin 2014, Yang *et al.* 2017, Liu *et al.* 2016, Namigata *et al.* 2016, Alaneme and Okotete 2016, Otsuka and Wayman 1998, Lu and Chen 2021, Velazquez and Romero 2020).

Most studies in the field of Cu-based SMAs have focused on Cu-Al-Ni, Cu-Zn-Al, and Cu–Al–Mn alloys because of their strong mechanical and magnetic properties that can be managed by chemical, mechanical and magnetic treatments (Titenko *et al.* 2020). CuAlMn shape memory alloys with a low degree of order of the $L2_1$ (Cu_2AlMn) phase that is situated within the composition range of the β single-phase (seen in Figs. 1 and 2) exhibit various interesting behaviors as compared to other Cu-based alloys (Kainuma *et al.* 1998, Velazquez and Romero 2020). These Heusler type shape memory alloys have excellent damping, one & two way SME, superelasticity, ferromagnetic, light-weight, and the Invar effect properties (Omori *et al.* 2007). Therefore, they are regarded as having high potential to be used in smart material applications in the future for their functional properties.

The studies on Heusler alloys were done firstly by F. Heusler in 1903 (Webster 1969) and he proclaimed that it was possible to obtain ferromagnetic alloys from non-ferromagnetic constituents Cu-Mn alloy and additional sp elements (Al, Sn, Sb etc.). Heusler alloys, defined as ternary intermetallic compounds, can have a composition of XYZ (named as half-Heuslers) or X_2YZ (named as full-Heuslers or fully ordered $L2_1$ structure), where X and Y refer to transition metals and Z stands for p-block metal elements (Webster 1969, Bradley and Rodgers 1934). In the condition of stoichiometric composition, full Heusler alloys (X_2YZ) crystallizes in $L2_1$ phase. CuAlMn alloy is also a kind of Heusler shape memory alloy (Cu_2AlMn) in which manganese sits at the body centers of the cubic $L2_1$ structure.

The addition of Mn content into the Cu-Al base system increases the allowable variation in composition (see in Fig. 2) for which SME is found (Omori *et al.* 2007). By doping Mn into binary CuAl alloys, the excellent ductility and strong superelasticity strain are obtained by manipulating grain size and texture (Titenko *et al.* 2020, Canbay *et al.* 2014b, Sutou *et al.* 2013, Sutou *et al.* 2008). The workability of these kinds of alloys is highly dependent on the ratio of Al, as the Al proportion is reduced, the alloy's workability rises significantly (Canbay *et al.* 2014a).
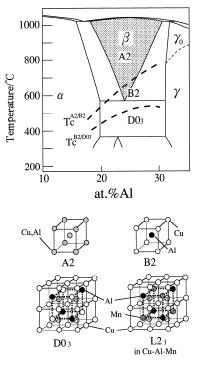
Fig. 1 Phase diagram of the Cu–Al alloy system showing the A2(disordered) → B2(ordered) → DO₃(or L2₁) transition temperatures (Liu *et al*.1998)
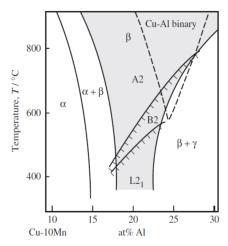

Fig. 2 Vertical section of 10 at% Mn in Cu-Al-Mn system with phase of Cu-Al binary system indicated by a broken line (Omori et al. 2007)

The binary Cu-Al-based SMAs, so the CuAlMn show themselves generally in the β phase at higher temperatures above the austenite phase start temperature (A$_s$) (Canbay *et al*. 2019, Otsuka and Wayman 1998, Velazquez and Romero 2020). By rapid cooling, this β phase converts to L2₁ (a type of DO₃ cubic superlattice) type of parent β1 austenite phase before the martensitic transformation

region that starts at austenite phase finish temperature (A_f) and ends at austenite starts temperature (A_s). During cooling from A_f to A_s temperature, the austenite (A) to martensite (M) transformation occurs isothermally and non-diffusional by the effect of internal stresses and it completesat A_s temperature. Similarly, by heating, the reverse martensitic transformation from M to A phase starts at M_s and ends up at M_f temperature. During these direct and reverse transformations, the average movement distance of the atoms of alloying elements in the crystal lattice is regarded as to be smaller than the lattice parameter and atoms move cooperatively in such movements. The martensitic transformation occurs by a shear-like mechanism and many martensite variants with different orientations form from the same parent austenite phase due to that martensite has low symmetry. At the end of martensitic transformation, different types of martensite phase forms such as $\alpha1'(6R)$, $\beta1'(18R)$, $\beta1''(18R+2H)$, and $\gamma1'(2H)$ can be formed depending on their chemical compositions, heating/cooling rate, application of stress and crystal orientations (Prado *et al*. 1995, Miyazaki 1996, Karaduman *et al*. 2019b, Sarı and Aksoy 2006). Where the capital letter of R refers to the rhombohedral (monoclinic M18R) and H refers to the hexagonal (orthorhombic superstructure of hcp) lattice types of stacking structures (Sarı and Aksoy 2006, Sluiter 2007).

In Cu-based alloys, depending on the number of close-packed layers in the unit cell, the internally faulted (or distorted) martensites are characterized by the long period stacking order types of 9R or 18R structures (Roh *et al*. 1992). In fact the 9R and 18R structures are bodily similar, except for a doubling of the unit cell in the b- and c-axis directions in the 18R case due to a variance occurs in transition from the B2 to $D0_3$ (or $L2_1$) phase. It was shown that these martensites can be formed in the normal orthorhombic (N9R or N 18R) or modified monoclinic (M9R or M18R) conditions, depending on the relative positions of the close-packed layers (Roh *et al*. 1992, Saburi *et al*. 1976). The difference in the N18R and M18R martensites stems from the stacking positions of the close-packed layers corresponding to the basal plane. In the M18R martensite, the relative displacement between two adjacent close-packed planes is deviated from their ideal positions.

The ternary addition of Mn element to the binary Cu-Al alloy refines the grain size, decrease and surpass aluminum's brittleness effect on the Cu-based alloy matrix (Sutou *et al*. 1999, Mallik and Sampath 2008, Karaduman *et al*. 2019a), and also increases the stability of the cubic β phase and widens the single-phase region which includes the $L2_1$ phase (Kainuma *et al*. 1998). The $L2_1$ austenite structure of Heusler CuAlMn memory alloy generally changes into a mixture of 18R($\beta1'$ or $\beta3'$) and 2H($\gamma1'$ or $\gamma3'$) martensites which one of these becomes volumetrically dominant on the other one depending on the percentage of Al and other additional contents and the ratio of the average conduction electron number per atom (e/a) (Sarı and Aksoy 2006, Ci *et al*. 2017, Mallik and Sampath 2008, Canbay *et al*. 2019, Velazquez and Romero 2020).

In this study, the ternary CuAlMn shape memory alloy with its unprecedented 69.71Cu-25.02Al-5.28Mn (at.%) composition produced by arc melting method. The SME properties of the new alloy were characterized by thermodynamic and microstructural measuring experiments and theoretical analysis.

2. Experimental

In this work, to prepare the ternary CuAlMn alloy with its unprecedented 69.71Cu-25.02Al-5.28Mn (at.%) composition by arc melting method (Canbay *et al*. 2019, Karaduman *et al*. 2019a, Velazquez and Romero 2020, Lu and Chen 2021). To do this, preliminarily the high purity (99.9 %) elements of Cu, Al, and Mn powders were mixed, then this powder mixture was pelletized under pressure. The pellets were melted in an Edmund Buehler Arc Melter under argon atmosphere and

the alloy was cast as ingot form. The most prominent reasons for using Edmund Buhler Arc Melter are because it has double-walled high vacuum chamber & pumping with back filling inert argon atmosphere to minimize oxidation during melting and measuring system, enables excellent observation of the melting process, so you can see when you (can) turn/mix over or remelt the material to improve homogenization without breaking the vacuum. Then this ingot was cut into small thin flat pieces (~40 mg and ~5×4×2 mm) to make better for the characterization tests and they were all solution-treated at 900°C for 1 h for atomic homogenization. After the end of the homogenization process, the alloy samples were immediately submerged (quenched) in the iced-brine water for cooling them fast. In this way, the formation of precipitations was minimized and thus the martensite phase was formed in the alloy samples. Then these samples underwent a series of measurements including differential scanning calorimetry (DSC), differential thermal analysis (DTA), energy dispersive X-ray spectrum (EDS), X-ray diffraction (XRD), optical microscopy and Vickers microhardness tests. To observe the heat induced martensitic transformation peaks on the thermal characteristic graphic (thermogram) of the alloy a Shimadzu DSC-60A instrument was used to take the DSC cycle at the heating/cooling of the rate of 10°C/min and liquid nitrogen (Shaw *et al.* 2008) was used to reach under room temperature. By using a Shimadzu DTG-60 AH, the DTA test was carried out at the rate of 25°C/min to observe the high-temperature behavior of the alloy. To determine the alloy's composition (at.%), a Bruker Model EDS instrument was used at room temperature, by which the alloy surface atoms were scanned topologically to determine the composition. To reveal the crystallographic features of the alloy by its X-ray diffraction pattern, a Rigaku RadB-DMAX II diffractometer with CuKα radiation was used at room temperature. The optical microscopy image (metallograph) of the alloy surface was taken by using an optical microscope model with no. XJP-6A at room temperature, which can take the micrometer sized images of the alloy surface morphology and can display the surface features of grain, grain boundaries, martensite phases and other formations. Furthermore, the mechanical features like the softness of the CuAlMn alloy were also examined by the Vickers microhardness test made by using a Tronic DHV 1000 model Digital Microhardness Tester under 100gf load at room temperature.

3. Results and discussions

The DSC curve of the CuAlMn alloy run at 10°C/min of heating/cooling rate is given as a cycled curve in Figs. 3(a) and (b) as we can notice from Fig. 3(a) (temperature on the x-axis) and the same curve (time on the x-axis) with peak analysis made by a tangent method which could be seen in Fig. 3(b). According to Fig. 3(a), on heating the alloy, there can be seen a down endothermic peak at around 80°C indicating a forward martensitic transformation from martensite (M) to austenite (A) phase (Canbay *et al.* 2019, Karaduman *et al.* 2019a, b) which was shown with M→A annotation above this peak in the figure. Then on cooling, there appears a backward A→M phase transformation around room temperature. There is also seen some fluctuations on the cooling part of the DSC curve before reaching the A→M transition peak and these happened due to the insertion of liquid nitrogen in the supplemental cooling port of the DSC instrument by which enabled the temperature of the alloy sample to be down under the room temperature.

The characteristic martensitic phase start and finish temperatures (A_s, A_f, M_s, M_f, A_{max}) of these two counterparts reversible martensitic peaks were determined by DSC peak analysis on the time axis seen in Fig. 3(b) and the peak areas, automatically calculated by the DSC analysis program, were appended above the peaks which shows the enthalpy changes ($\Delta H_{M \to A}$ and $\Delta H_{A \to M}$) occurred

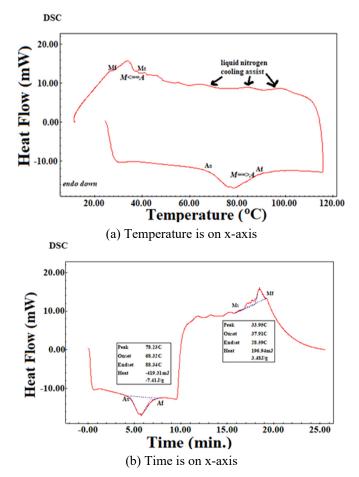(a) Temperature is on x-axis

(b) Time is on x-axis

Fig. 3 DSC curve of Cu-Al-Mn alloy at the heating/cooling rate of 10 °C/min. In the analysis boxes, 'Onset' and 'Endset' are peak/phase start and finish temperatures. Also, the values of the enthalpy changes (J/g) that occurred during these phase transformations are given at the bottom of the boxes

Table 1 Transformation temperatures and kinetic parameters of CuAlMn alloy at 10°C/min of heating/ cooling rate

A_s (°C)	A_f (°C)	M_s (°C)	M_f (°C)	A_s-M_f (°C)	T_0 (°C)	$\Delta H_{M \rightarrow A}$ (J/g)	$\Delta H_{A \rightarrow M}$ (J/g)	$\Delta S_{M \rightarrow A}$ (J/g°C)	$\Delta S_{A \rightarrow M}$ (J/g°C)
68.32	88.34	37.91	28.59	39.73	63.12	7.41	-3.48	0.1174	-0.0551

during these transformations. The values of these thermodynamical parameters plus the calculated others such as hysteresis (A_s-M_f) value, equilibrium temperature (T_o), and entropy change amounts ($\Delta S_{M \rightarrow A}$ and $\Delta S_{A \rightarrow M}$) were all listed in Table 1.

The equilibrium temperature (T_0) is the temperature at between M_s and A_s temperatures where the chemical Gibbs free energies of the two phases are equal. The T_0 temperature was calculated by $T_0 = (A_f + M_s) \times 0.5$ relation of Tong-Wayman (Tong and Wayman 1974). ΔS entropy change values

were calculated by using $\Delta S_{A \leftrightarrow M} = \Delta H_{A \leftrightarrow M}/T_0$ formula (Canbay *et al.* 2019, Karaduman *et al.* 2019a) for each opposite way transformation.

The DTA measurement for the alloy was taken at the heating/cooling rate of 25°C/min and given in Fig. 4. As to this DTA cycle, on heating (on the down part of the DTA curve), the CuAlMn alloy underwent a series of transitions as β3(DO$_3$; L2$_1$) → β2(B2, metastable) → α+γ2 precipitating → eutectoid reaction → β2(B2, ordered) → β(A2, disordered) and this thermal pattern was found compatible with the previous literature works (Karaduman *et al.* 2019a, b, Prado *et al.* 1995, Velazquez and Romero 2020). There appeared also a small exo-peak that raised at the end of cooling process (on the far left of the upper part of the DTA curve at around room temperature, and this DTA test was taken on a hot summer day, the test lab's ambient temperature was around 35°C) which therefore indicates an incomplete A→M transition that occurred there. The reason for no any endo-peak indicating the M→A transition on the far left of the bottom heating part of the curve is due to that alloy sample was already in the austenite phase when DTA heating was started (because another piece of alloy sample in the austenite phase was used for DTA test).
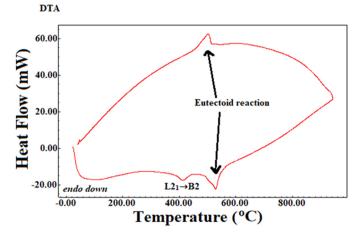

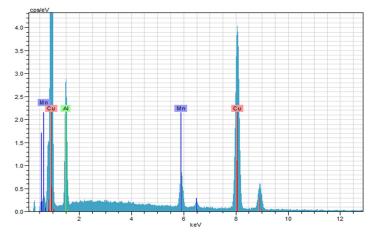Fig. 4 DTA curve of CuAlMn alloy at the heating/cooling rate of 25°C/min

Fig. 5 The EDS result of CuAlMn alloy

The chemical composition of the CuAlMn alloy was determined by the EDS test taken at room temperature and the EDS result is given in Fig. 5. The existence of Cu, Al, and Mn constituent elements was detected.

The average valence electron concentration per atom (e/a) is an important parameter for the alloys in terms of having SME property. Moreover, the vibrational entropy change (ΔS) of the average periodic lattice formation emerges during the first order and non-diffusional martensitic transformations depend considerably on this parameter (Ahlers 1995). Cu-based SMAs generally have SME property when their e/a values are between ~1.45 and 1.50 (Otsuka and Wayman 1998, Canbay *et al*. 2019, Velazquez and Romero 2020). In this e/a value interval, the martensite phases of monoclinic β1′ (or β3′; M18R) and hexagonal close-packed γ1′ (or γ3′; 2H) together take place (Canbay *et al*. 2019). The 18R martensite becomes the dominant martensite form for the e/a values lower than 1.45 and inversely for the values larger than 1.50, at this time the 2H martensite phase gains dominancy (Canbay *et al*. 2019). Therefore, determining the e/a value of an alloy can give a theoretical prediction on which martensite phase types are formed in the alloy matrix. Here, the value of e/a ratio of the CuAlMn SMA was found as 1.55 by using $e/a = \sum f_i v_i$ formula (Canbay *et al*. 2019), where; f_i represents the atomic fractions of alloying elements and v_i is their valence numbers. This value is close to the interval of 1.45-1.50 and larger than 1.50, therefore it can be expected that the 18R and 2H martensite forms will be together in the CuAlMn alloy matrix, with a slight dominancy of 2H form. The X-ray diffraction pattern and optical microscopy image of the CuAlMn alloy that is given ahead confirm this prediction.

On the optical microscopy images given in Fig. 6 that display the surface morphology of the CuAlMn alloy, the wedge-like and V-type monoclinic β3′(M18R), the coarse γ3′(2H) type (the dark-lighted strips) martensite forms can be clearly seen (Agrawal and Vajpai 2020, Al-Humairi 2019, Li *et al*. 2020).

The result of the XRD measurement taken at room temperature for the CuAlMn alloy sample can be seen in Fig. 7. On this X-ray diffraction pattern, the highest peak of (012) plane belongs to the γ1′(or γ3′) hexagonal martensite and then secondly γ1′(211), and the other peaks are β1′(1210), β1′(2010), β1′(122), β1′(0022) and β1′(042) that belong to the monoclinic β1′(β3′) martensite phase (Canbay *et al*. 2014a, Braga *et al*. 2017, Li *et al*. 2020). These XRD peaks that show the existence of the 18R(β1′) martensite together with the dominant 2H(γ1′) martensite in the CuAlMn alloy, so
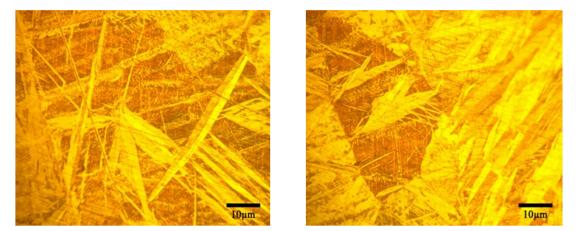

Fig. 6 The optical microscopy images of the CuAlMn alloy displaying the surface morphology of the alloy
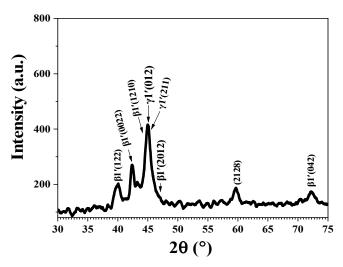
Fig. 7 The X-ray diffraction pattern of the Cu-Al-Mn alloy

the results of both XRD and optical microscopy confirm the aforementioned theoretical prediction deduced on the value of *e*/*a* ratio of the alloy.

Another important structural parameter of the alloy is the average crystallite size (D) which can be determined by using XRD data. The coherently X-ray scattering domain (spherical or ellipsoidal particle) size is the Debye-Scherrer (Patterson 1939) crystallite size and it is generally in sub-micrometer scale and is smaller than the micrometer sized grains. For the produced CuAlMn alloy, the value of the D size refers to the coherently X-ray scattering domain size of β1′ martensite phase in this alloy. A larger D value indicates a larger single-like crystallinity i.e., a better shape memory effect (Canbay *et al*. 2019). The lattice impurities, imperfections, stacking faults, grain boundaries, crystallite smallness, chemical heterogeneities etc. reduce the X-ray scattering domain size (D size) i.e., such defects increase amorphism in the alloy and shows itself by broadened peaks on the X-ray pattern. There is a relation between the size of nano-scale crystallites in a solid and the broadening of a peak in the diffraction pattern and is expressed by Debye-Scherrer formula $D = 0.9\lambda/B_{1/2}\cos\theta$ (Canbay *et al*. 2019), where; λ refers to the X-ray wavelength of the CuKα radiation ($\lambda = 0.15406$ nm), $B_{1/2}$ is full width at half maximum (FWHM) value of the highest peak (= 0.375), and θ is its diffraction Bragg angle (= 44.958°). The average crystallite size (D) value of the alloy was calculated as 22.93 nm (Canbay *et al*. 2019, Karaduman *et al*. 2019a).

The Vickers microhardness value of the CuAlMn alloy was obtained as 230.33 HV from taking the average on three different region values of 244 HV 237 HV and 210 HV. The microhardness values of CuAlMn alloy showed the high ductility aspect of the CuAlMn alloy and these values were also found in a good agreement with the slightly higher values reported in a previous CuAlMn SMA work (Oliveira *et al*. 2016).

4. Conclusions

The ternary CuAlMn shape memory Heusler alloy was fabricated successfully by arc melting method and characterized by thermal (DSC, DTA), mechanical (Vickers microhardness) and structural (XRD, EDX) measurements. By these measurements that we listed below, the presence of

the shape memory effect property of the CuAlMn alloy was demonstrated.

- The martensitic transformation temperatures were detected in the temperature range between 28°C and 88°C by DSC test that indicates a SME property. The multiple phase transitions of L2$_1$ → B2 → α+γ2 → eutectoid reaction → B2 → A2, which is the common thermal behavior of Cu-based Heusler shape memory alloys, was observed on the DTA curve.
- The structural tests and the theoretical predictions made on the calculated average valence electron concentration of the alloy, both indicated the existence and dominancy of 18R and 2H martensite forms, were found in good accordance.
- Mechanical low microhardness values of the alloy that was found slightly smaller than the values in a previous report (Oliveira *et al*. 2016) implied high softness or ductility feature of the produced alloy.

Acknowledgments

References

Agrawal, A. and Vajpai, S.K. (2020), "Preparation of Cu-Al–Ni shape memory alloy strips by spray deposition-hot rolling route", *Mater. Sci. Technol.*, **36**(12), 1337-1348. https://doi.org/10.1080/02670836.2020.1781354
Ahlers, M. (1995), "Phase stability of martensitic structures", *J. De Phy IV*, **5**(C8), C8-C71-8-80. https://doi.org/10.1051/jp4:1995808
Alaneme, K.K. and Okotete, E.A. (2016), "Reconciling viability and cost-effective shape memory alloy options – A review of copper and iron based shape memory metallic systems", *Eng. Sci. Technol.*, **19**(3), 1582-1592. https://doi.org/10.1016/j.jestch.2016.05.010
Al-Humairi, S.N.S. (2019), "Cu-based shape memory alloys: modified structures and their related properties", Book Chapter in: *Recent Advancements in the Metallurgical Engineering and Electrodeposition*, IntechOpen Ltd., London, UK. https://doi.org/10.5772/intechopen.86193
Bradley, A.J. and Rodgers, J.W. (1934), "The crystal structure of the heusler alloys", *Proceedings of the royal society of london. Series A, Containing Papers of a Mathematical and Physical Character*, **144**(852), 340-359. http://doi.org/10.1098/rspa.1934.0053
Braga, F.D.O., Matlakhov, A.N., Matlakhova, L.A., Monteiro, S.N. and Araújo, C.J.D. (2017), "Martensitic transformation under compression of a plasma processed polycrystalline shape memory CuAlNi Alloy", *Mater. Res.*, **20**(6), 1579-1592. http://dx.doi.org/10.1590/1980-5373-MR-2016-0476
Canbay, C.A. and Aydoğdu, A. (2013), "Thermal analysis of Cu-14.82 wt% Al-0.4 wt% Be shape memory alloy", *J. Therm. Anal. Calorim.*, **113**, 731-737. https://doi.org/10.1007/s10973-012-2792-6
Canbay, C.A. and Karagoz, Z. (2013), "Effects of annealing temperature on thermomechanical properties of Cu–Al–Ni shape memory alloys", *Int. J. Thermophys.*, **34**, 1325-1335. https://doi.org/10.1007/s10765-013-1486-z
Canbay, C.A. and Keskin, A. (2014), "Effects of vanadium and cadmium on transformation temperatures of Cu–Al–Mn shape memory alloy", *J. Therm. Anal. Calorim.*, **118**, 1407-1412. https://doi.org/10.1007/s10973-014-4034-6
Canbay, C.A., Genc, Z.K. and Sekerci, M. (2014a), "Thermal and structural characterization of Cu–Al–Mn–X (Ti,Ni) shape memory alloys", *Appl. Phys. A*, **115**, 371-377. https://doi.org/10.1007/s00339-014-8383-6
Canbay, C.A., Ozgen, S. and Genc, Z.K. (2014b), "Thermal and microstructural investigation of Cu–Al–Mn–

Mg shape memory alloys". *Appl. Phys. A*, **117**, 767-771 https://doi.org/10.1007/s00339-014-8643-5

Canbay, C.A., Karaduman, O., Ünlü, N., Baiz, S.A. and Ozkul, İ. (2019), "Heat treatment and quenching media effects on the thermodynamical, thermoelastical and structural characteristics of a new Cu-based quaternary shape memory alloy", *Compos. Part B*, **174**(106940), 1-10. https://doi.org/10.1016/j.compositesb.2019.106940

Ci, W.Y., Abu Bakar, T.A., Hamzah, E. and Saud, S.N. (2017), "Study of X-phase formation on Cu-Al-Ni shape memory alloys with Ti Addition", *J. Mech. Eng. Sci.*, **11**(2), 2770-2779. https://doi.org/10.15282/jmes.11.2.2017.17.0251

Kainuma, R., Satoh, N., Liu, X.J., Ohnuma, I. and Ishida, K. (1998), "Phase equilibria and Heusler phase stability in the Cu-rich portion of the Cu–Al–Mn system", *J. Alloys Compounds*, **266**(1-2), 191-200. https://doi.org/10.1016/S0925-8388(97)00425-8

Karaduman, O., Canbay, C.A., Özkul, İ., Baiz, S.A. and Ünlü, N. (2019a), "Production and Characterization of Ternary Heusler Shape Memory Alloy with A New Composition", *J. Mater. Electron. Devices*, **1**(1), 16-19. Retrieved from http://www.dergi-fytronix.com/index.php/jmed/article/view/24

Karaduman, O., Canbay, C.A., Ünlü, N. and Özkul, İ. (2019b), "Analysis of a newly composed Cu-Al-Mn SMA showing acute SME characteristics", *AIP Conference Proceedings*, **2178**, 030039. https://doi.org/10.1063/1.513543

Li, H., Wang, Q., Yin, F., Cui, C., Hao, G., Jiao, Z. and Zheng, N. (2020), "Effects of Parent Phase Aging and Nb Element on the Microstructure, Martensitic Transformation, and Damping Behaviors of a Cu–Al–Mn Shape Memory Alloy", *Phys. Status Solidi A*, **217**, 1900923. https://doi.org/10.1002/pssa.201900923

Liu, X.J., Ohnuma, I., Kainuma, R. and Ishida, K. (1998), "Phase equilibria in the Cu-rich portion of the Cu–Al binary system", *J. Alloys Compounds*, **264**(1-2), 201-208. https://doi.org/10.1016/S0925-8388(97)00235-1

Liu, J.L., Huang, H.Y. and Xie, J.X. (2016), "Effects of aging treatment on the microstructure and superelasticity of columnar-grained Cu71Al18Mn11 shape memory alloy", *Int. J. Miner. Metall. Mater.*, **23**, 1157-1166. https://doi.org/10.1007/s12613-016-1335-8

Lu, N.H. and Chen, C.H. (2021), "Inhomogeneous martensitic transformation behavior and elastocaloric effect in a bicrystal Cu-Al-Mn shape memory alloy", *Mater. Sci. Eng.: A*, **800**, 140386. https://doi.org/10.1016/j.msea.2020.140386

Mallik, U.S. and Sampath, V. (2008), "Influence of aluminum and manganese concentration on the shape memory characteristics of Cu–Al–Mn shape memory alloys", *J. Alloys Compounds*, **459**(1-2), 142-147. https://doi.org/10.1016/j.jallcom.2007.04.254

Miyazaki, S. (1996), "Development and Characterization of Shape Memory Alloys", In: *Shape Memory Alloys*, International Centre for Mechanical Sciences (Courses and Lectures), Volume 351, p. 69-147, Springer, Vienna, Austria. https://doi.org/10.1007/978-3-7091-4348-3_2

Namigata, Y., Hattori, Y., Khan, M.I., Kim, H.Y. and Miyazaki, S. (2016), "Enhancement of shape memory properties through precipitation hardening in a Ti-rich Ti-Ni-Pd high temperature shape memory alloy", *Mater. Transact.*, **57**(3), 241-249. https://doi.org/10.2320/matertrans.MB201516

Oliveira, J.P., Panton, B., Zeng, Z., Omori, T., Zhou, Y., Miranda, R.M. and Fernandes, F.B. (2016), "Laser welded superelastic Cu–Al–Mn shape memory alloy wires", *Mater. Des.*, **90**, 122-128. http://dx.doi.org/10.1016/j.matdes.2015.10.125

Oliveira, J.P., Crispim, B., Zeng, Z., Omori, T., Fernandes, F.B. and Miranda, R.M. (2019), "Microstructure and mechanical properties of gas tungsten arc welded Cu-Al-Mn shape memory alloy rods", *J. Mater. Processing Tech.*, **271**, 93-100. https://doi.org/10.1016/j.jmatprotec.2019.03.020

Omori, T., Koeda, N., Sutou, Y., Kainuma, R. and Ishida, K. (2007), "Superplasticity of CuAl-Mn-Ni shape memory alloy", *Mater. Transact.*, **48**(11), 2914-2918. https://doi.org/10.2320/matertrans.D-MRA2007879

Otsuka, K. and Wayman, C.M. (1998), *Shape Memory Materials*, Cambridge University Press, Cambridge, UK.

Özkul, İ., Kurgun, M.A., Kalay, E., Canbay, C.A. and Aldaş, K. (2019), "Shape memory alloys phenomena: classification of the shape memory alloys production techniques and application fields", *Eur. Phys. J. Plus*, **134**, 585. https://doi.org/10.1140/epjp/i2019-12925-2

Patterson, A.L. (1939), "The Scherrer formula for X-ray particle size determination", *Phys. Rev.*, **56**(10), 978. https://doi.org/10.1103/PhysRev.56.978

Prado, M.O., Decorte, P.M. and Lovey, F. (1995), "Martensitic transformation in Cu-Mn-Al alloys", *Scripta Metallurgica et Materialia*, **33**(6), 877-883. https://doi.org/10.1016/0956-716X(95)00292-4

Roh, D.W., Lee, E.S. and Kim, Y.G. (1992), "Effects of ordering type and degree on monoclinic distortion of 18R-type martensite in Cu-Zn-Al alloys", *Metall. Transact. A*, **23**(10), 2753-2760. https://doi.org/10.1007/BF02651754.

Saburi, T., Nenno, S., Kato, S. and Takata, K. (1976), "Configurations of martensite variants in Cu-Zn-Ga", *J. Less Common Metals*, **50**(2), 223-236. https://doi.org/10.1016/0022-5088(76)90162-4

Sarı, U. and Aksoy, İ. (2006), "Electron microscopy study of 2H and 18R martensites in Cu–11.92wt% Al–3.78wt% Ni shape memory alloy", *J. Alloys Compounds*, **417**(1-2), 138-142. https://doi.org/10.1016/j.jallcom.2005.09.049

Shaw, J., Churchill, C. and Iadicola, M. (2008), "Tips and tricks for characterizing shape memory alloy wire: part 1—differential scanning calorimetry and basic phenomena", *Experim. Techniques*, **32**, 55-62. https://doi.org/10.1111/j.1747-1567.2008.00410.x

Sluiter, M.H.F. (2007), "Some observed bcc, fcc, and hcp superstructures", *Phase Transitions*, **80**(4-5), 299-309. https://doi.org/10.1080/01411590701228562

Sutou, Y., Kainuma, R. and Ishida, K. (1999), "Effect of alloying elements on the shape memory properties of ductile Cu–Al–Mn alloys", *Mater. Sci. Eng. A*, **273-275**, 375-337. https://doi.org/10.1016/S0921-5093(99)00301-9

Sutou, Y., Omori, T., Kainuma, R. and Ishida, K. (2008), "Ductile Cu–Al–Mn basedshape memory alloys: general properties and applications", *Mater. Sci. Technol.*, **24**(8), 896-901. https://doi.org/10.1179/174328408X302567

Sutou, Y., Omori, T., Kainuma, R. and Ishida, K. (2013), "Grain size dependence of pseudoelasticity in polycrystalline Cu–Al–Mn-based shape memory sheets", *Acta Materialia*, **61**(10), 3842-3850. https://doi.org/10.1016/j.actamat.2013.03.022

Titenko, A., Demchenko, L., Perekos, A., Babanli, M., Huseynov, S. and Ren, T.Z. (2020), "Deformational and magnetic effects in Cu–Al–Mn alloys", *Appl. Nanosci.*, **10**(12), 5037-5043. https://doi.org/10.1007/s13204-020-01494-9

Tong, H.C. and Wayman, C.M. (1974), "Characteristic temperatures and other properties of thermoelastic martensites", *Acta Metall.*, **22**, 887-896. https://doi.org/10.1016/0001-6160(74)90055-8

Velazquez, D. and Romero, R. (2020), "Calorimetric study of spinodal decomposition in β-Cu–Al–Mn", *J. Therm. Anal. Calorim.*, 1-7. https://doi.org/10.1007/s10973-019-09234-0

Webster, P.J. (1969), "Heusler alloys", *Contemporary Phys.*, **10**(6), 559-577. https://doi.org/10.1080/00107516908204800

Xie, J., Liu, J. and Huang, H. (2015), "Structure design of high-performance Cu-based shape memory alloys", *Rare Met.*, **34**, 607-624. https://doi.org/10.1007/s12598-015-0557-7

Yang, S., Zhang, F., Wu, J., Lu, Y., Shi, Z., Wang, C. and Liu, X. (2017), "Superelasticity and shape memory effect in Cu–Al–Mn–V shape memory alloys", *Mater. Des.*, **115**, 17-25. https://doi.org/10.1016/j.matdes.2016.11.035

CC